Hynek Řezníček; Jan Geletič; Martin Bureš; Pavel Krč; Jaroslav Resler; Kateřina Vrbová; Arsenii Trush; Petr Michálek; Luděk Beneš; Matthias Sühring

Different boundary conditions for LES solver Palm 6.0 used for ABL in tunnel experiment

In: Jan Chleboun and Pavel Kůs and Jan Papež and Miroslav Rozložník and Karel Segeth and Jakub Šístek (eds.): Programs and Algorithms of Numerical Mathematics, Proceedings of Seminar. Jablonec nad Nisou, June 19-24, 2022. Institute of Mathematics CAS, Prague, 2023. pp. 209–218.

Persistent URL: http://dml.cz/dmlcz/703201

Programs and Algorithms of Numerical Mathematics 21
J. Chleboun, P. Kůs, J. Papež, M. Rozložník, K. Segeth, J. Šístek (Eds.)
Institute of Mathematics CAS, Prague 2023

DIFFERENT BOUNDARY CONDITIONS FOR LES SOLVER PALM 6.0 USED FOR ABL IN TUNNEL EXPERIMENT

Hynek Řezníček[1,3], Jan Geletič[1], Martin Bureš[1], Pavel Krč[1], Jaroslav Resler[1], Kateřina Vrbová[2], Arsenii Trush[2], Petr Michálek[2], Luděk Beneš[3], Matthias Sühring[4]

[1] Institute of Computer Science, Czech Academy of Sciences, Prague (cs.cas.cz - reznicek@cs.cas.cz)
[2] Institute of Theoretical and Applied Mechanics, Czech Academy of Sciences, Prague (itam.cas.cz)
[3] Faculty of Mechanical Engineering, Czech Technical University in Prague (fs.cvut.cz)
[4] Institute of Meteorology and Climatology, Leibniz University in Hanover (meteo.uni-hannover.de)

Abstract: We tried to reproduce results measured in the wind tunnel experiment with a CFD simulation provided by numerical model PALM. A realistic buildings layout from the Prague-Dejvice quarter has been chosen as a testing domain because solid validation campaign for PALM simulation of Atmospheric Boundary Layer (ABL) over this quarter was documented in the past. The question of input data needed for such simulation and capability of the model to capture correctly the inlet profile and its turbulence structure provided by the wind-tunnel is discussed in the study.
The PALM dynamical core contains a solver for the Navier-Stokes equations. By default, the model uses the Large Eddy Simulation (LES) approach in which the bulk of the turbulent motions is explicitly resolved. It is well validated tool for simulations of the complex air-flow within the real urban canopy and also within its reduced scale provided by wind tunnel experiments. However the computed flow field between the testing buildings did not correspond well to the measured wind velocity in some points. Different setting of the inlet boundary condition was tested but none of them gave completely developed turbulent flow generated by vortex generators and castellated barrier wall place at the entrance of the aerodynamic section of the wind tunnel.

Keywords: large eddy simulation, wind tunnel, atmospheric boundary layer, PALM model, turbulence

MSC: 65Z05, 86A10, 76F65

DOI: 10.21136/panm.2022.19

1. Introduction

PALM model is capable to simulate turbulent air-flow within the lowest part of the ABL. By default, it uses the LES approach in which the bulk of the turbulent motions is explicitly resolved [4]. The core was already validated according to tunnel measurements in [2], therefore our expectations were high.

The realistic buildings layout from Prague-Dejvice quarter is chosen as the testing domain. The choice of this particular domain is motivated by existing validation for the PALM model in Dejvice quarter [5]. The same domain was 3D-printed and placed to the test section of the wind tunnel in Telč (Vincenc Strouhal) owned by ITAM which calibration is documented in [3]. To achieve the flow similar to real ABL in reduced scale the wind tunnel used three elements of the turbulence generation - vortex spikes and castellated barrier wall before the atmospheric section and roughness elements inside the atmospheric section (before the model test section).

Originally we were interested to model the influence of passageways inside the buildings on the flow field in courtyards and we wanted to compare our numbers to ones measured in the tunnel by 5-holes probe. The inconsistency in the results for the base-case forced us to study the problem how to correctly reproduce the well defined but still vaguely described (in a certain sense) flow field in the wind tunnel's atmospheric test section.

The question should be which data and in which form are needed from the measurement (or calibration) for the CFD models to set the inflow properly.

2. Mathematical model

The simulated air is considered as incompressible (due to much lower velocities in comparison to the speed of sound), viscid (the molecular viscosity is neglected everywhere except for the turbulent dissipation) and neutrally stratified (for testing the dynamical core only without unfavourable stratification effects) gas.

The dynamical core of PALM model is based on Navier-Stokes equations in Boussinesq approximation for filtered quantities (filtering usually denoted with overbar is omitted here due to readability)

$$\begin{aligned} \nabla \cdot \mathbf{u} &= 0 \\ \frac{\partial \mathbf{u}}{\partial t} + (\mathbf{u} \cdot \nabla)\mathbf{u} &= -\frac{1}{\rho_0}\nabla\pi + \mathbf{g} - \nabla \cdot \underline{\underline{\boldsymbol{\tau}}} \end{aligned} \tag{1}$$

The velocity vector $\mathbf{u} = u_i = (u, v, w)$ describes the movement of air which is assumed to be dry with constant density $\rho_0 = 1\ \mathrm{kg/m^3}$. The gravitational acceleration denoted as $\mathbf{g} = -g\delta_{i3}$ is acting only in vertical direction (here written using Kronecker's delta δ_{ij} in third component), its value is set to $g = 9.81\ \mathrm{m/s^2}$. The modified pressure fluctuation can be expressed as $\pi = p + \frac{2}{3}\rho_0 e$ using the pressure fluctuation p and sub-grid-scale (sgs = unresolved) turbulent kinetic energy e. The residual stress tensor $\underline{\underline{\boldsymbol{\tau}}} = \tau_{ij}$ symbolises the turbulent part of the flow.

The modified Deardorff's model is employed for turbulent closure (written in Einstein summation convention follows)

$$\begin{aligned} \tau_{ij} = \overline{u_i'' u_j''} - \frac{2}{3} e \delta_{ij} &= -K_m \left(\frac{\partial u_i}{\partial x_j} + \frac{\partial u_j}{\partial x_i} \right) \\ \frac{\partial e}{\partial t} + u_j \frac{\partial e}{\partial x_j} &= 2K_m \nabla^2 e + \overline{u_i'' u_j''} \frac{\partial u_i}{\partial x_j} - \epsilon \end{aligned} \tag{2}$$

A double prime indicates sgs velocities, the overbar indicating filtering is added for the sgs flux terms. The local (sgs) eddy diffusivity coefficient of momentum K_m is approximated as $K_m \approx 0.1\Delta\sqrt{e}$, where distance $\Delta = \min\{\Delta_{x_i}\}$ is minimal grid spacing. This distance serves also as implicit filter for large eddies. The dissipation rate is approximated as $\epsilon \approx 0.93\frac{\sqrt{e^3}}{\Delta}$. For more details please see the documentation in [4]. Further the dimensions are referenced as $x_i = (x, y, z)$.

2.1. Numerical solver

The equations are spatially discretized by using finite differences at equidistant horizontal grid spacing while the vertical grid is stretched above the surface layer to save CPU-time. The stretching factor applied above 100 m height set to 1.01 is limited by maximal vertical step ($\max \Delta_z = 2\Delta_x$). Arakawa staggered C-grid is used for velocity **u** defined at edges of the grid cell while the scalars are defined in the grid cell center (see Fig. 1). The Upwind-biased 5^{th} order advection scheme based on flux formulation according to [6] is used.

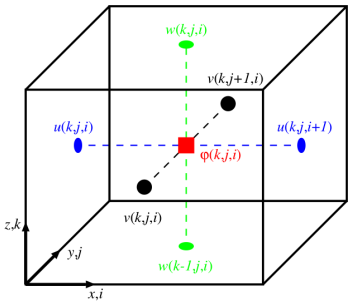

Fig. 1: Arakawa staggered C-grid [4]

The time integration is done by 3^{rd} order low-storage (3 stages) Runge-Kutta method according to [1]. It is proved that the CFL condition in such case can be $C_{\mathrm{CFL}} = \frac{\max_i\{u_i\}\Delta_t}{\Delta} < 1.4$ which limits the maximal time step Δ_t.

To enforce incompressibility (divergence free velocity field needed by Bouissinesq approx.) a predictor-corrector method is used where Poisson equation is solved for the modified perturbation pressure (π) after every time step. The resulting system of linear equations is solved with Gauss-Seidel method and multi-grid scheme is employed if number of cells per core is even . The detailed description can be found in [4].

3. Set-up and boundary conditions

As mentioned above, the measurement was done in wind tunnel at the ITAM in Telč, detailed description can be found in [3] and mentioned references. What is important to notice here is the arrangement of elements generating the ABL flow before the aerodynamic test section as can be seen in the Fig. 2, because the castellated barrier wall and vortex generators are not a part of the numerically modeled

domain. Their placement to the numerical domain close to the inlet would caused a significant extension of the domain and therefore slowing down the computations.

The real world building configuration in Prague-Dejvice between streets Jugoslavskych partyzanu and Terronska was chosen as testing area (serves as inner domain in the model). The Fig. 3 shows the map of the area with blue circle indicating the passage-way in the building in Rooseveltova street. The area is rotated clockwise to adjust the air flow with x-direction. The situation in the test section (inner domain in the model) is shown in the Fig. 4 with marked measuring point locations.

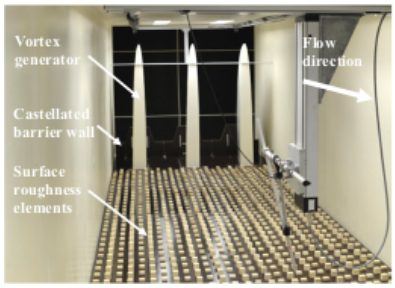

Fig. 2: View from the aerodynamic test section backwards (against the flow).

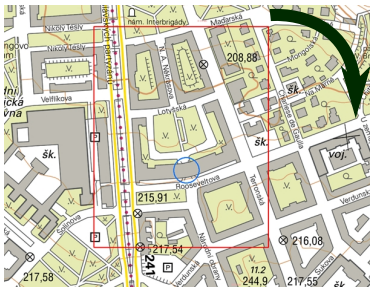

Fig. 3: Map of chosen area. The domain is rotated clockwise in the model.

Fig. 4: The same area as inner domain with measuring points.

The scale of the model is 1:300 which holds for time and space meaning that the 1 min. average in the tunnel is 5 hours average in real. A characteristic length is chosen as the height of the vortex generator which is $H = 1.5$ m in the tunnel which corresponds to 450 m in reality. The advantage of the scale setting is that the velocities can be compared 1:1. If the reference velocity $U_{\text{ref}} = 6.6$ m/s is considered, the Reynolds number in the tunnel is $Re \approx 10^6$ which is large enough. If Townsend's hypothesis applies, the flow in the wind tunnel should be dynamically comparable to the real one. The computational domain contains all the roughness elements (simulated directly) as can be seen in the Fig. 5. The whole domain 3000×600 m large includes the test section with dimensions 600×500 m (all listed as real here). The resolution of the grid is set to $\Delta = 1$ m.

The wind tunnel measurements were performed using five-hole fast response pressure probe "Cobra" with integrated pressure-to-voltage transducers. The probe was mounted on a traversing device that could move it in all three directions x, y, z, see Fig. 2 right. The used sampling frequency was 1000 Hz and sampling time was 60 s for each measuring record. The probe records evaluations were made in MATLAB with the use of routines and calibrations from the probe manufacturer, Aeroprobe Corporation.

The wind velocity and Turbulent Intensity (TI) profiles measured by a hot-wire above the roughness elements (before the inner domain) were available from the validation article [3]. For this study the profiles measured before the inner domain

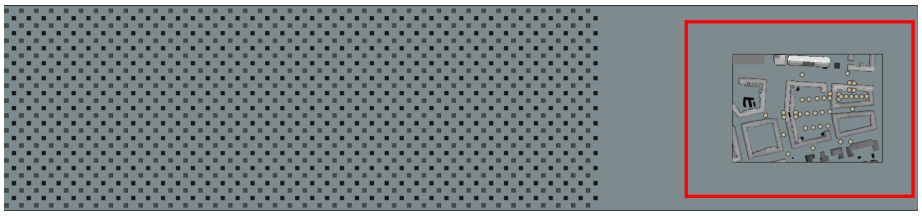

Fig. 5: Computational domain with buildings in the test section (marked in red).

are important, specially profile measured at the beginning of inner domain and profile measured approximately one meter before inner domain. The maximal height of the profiles is 0.47H and the height of our simulation domain was chosen accordingly (the height of the wind tunnel channel is 1.3H). The values for the profiles were taken from wind tunnel validation measurement provided in [3] since the measurement of these profiles during our experiment wasn't accomplished.

3.1. Boundary conditions

The boundary conditions (b.c.) are set as follows:

On **inlet** the vertical velocity profile driven by $U_{\text{ref}} = 6.6$ m/s is prescribed for the first velocity component $u = u(z)$ profile (different profiles were tested - uniform, logarithmic and power law) with statistically created disturbances every 60 s with amplitude ± 0.25 m/s from the mean velocity. The other components are set to $v = w = 0$. Homogeneous (homog.) Neumann b.c. is prescribed for the other quantities (e, p).

On **outlet** a radiation b.c. [4] is used for all velocity components where a constant phase velocity is considered as maximum value allowed by CFL condition. Homog. Neumann condition is assumed for scalar quantities (e, p).

At the **bottom** homog. Dirichlet b.c. for velocity vector $\mathbf{u}(0) = \mathbf{0}$ (no slip) is used. Homog. Neumann b.c. is prescribed for the other quantities (e, p).

At the **top** boundary Dirichlet b.c. for the first velocity component is given by the inlet profile as $u(z_{\max}) = \max u(z)$. For the other components and the pressure perturbation the homog. Dirichlet b.c. is utilized. Homog. Neumann condition is assumed for sgs-tke (e).

On **sides** the cyclic b.c. is prescribed for all quantities.

4. Results

The whole aerodynamic section (including the roughness elements in front of the test section) of the wind tunnel was simulated and the results were compared to the measurements. The main comparison was done for velocity components in the given points (see Fig. 4) obtained by five-hole probe for three different heights: 3, 10

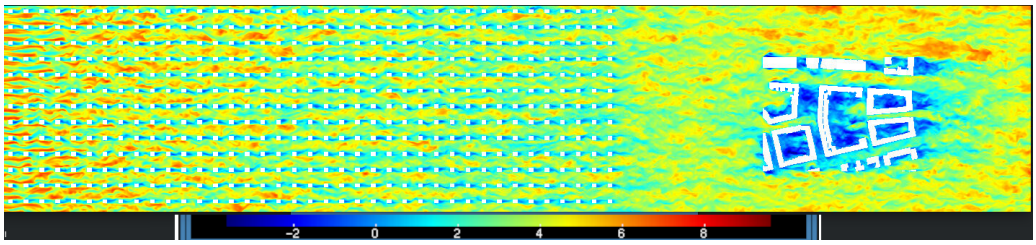

Fig. 6: Horizontal velocity field in $z = 9$ m captured after 1 hour simulation (u - instantaneous values).

and 30 m (listed as real dimensions). Nevertheless, the agreement of the velocity and turbulent intensity profiles measured by hot-wire probe in the tunnel axes in front of the test section was also important.

The first numerical experiment was performed with uniform inlet velocity profile $u(z) = U_{\text{ref}}$ and was considered as naive attitude serving as technical preview. The flow was decelerated and its turbulent intensity was increased within the roughness elements section. The example of such horizontal velocity field (u) in 9 m height captured in a moment when the simulation time hits 1 hour is shown in the Fig. 6.

The model outputs were mainly saved every 30 minutes as time averages and then their mean over 5 hours simulation were computed. Example of such output for velocity component u in the test section is rendered in the Fig. 7. There, one can easily identify the influences of the buildings and their recirculation zones. Also, the influence of the passageway is identified in the middle of the U-shaped building which allows some air to go through. Therefore the flow behind the passageway is faster than the flow in the surrounding area.

The hit ratio for velocity magnitudes displayed in the Fig. 8 shows the discrepancy between model and experimental results. The values given by the model are seriously under-predicted in most points (somewhere more than by 25% - as indicate the lower green line). The reason probably lies in wrong velocity profile at the entrance of the

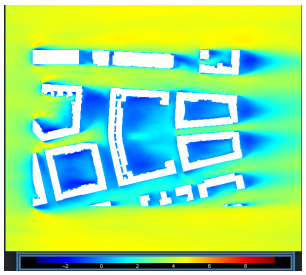

Fig. 7: 30 minutes average for u, in $z = 9$ m, $t = 1$ h (In the test section).

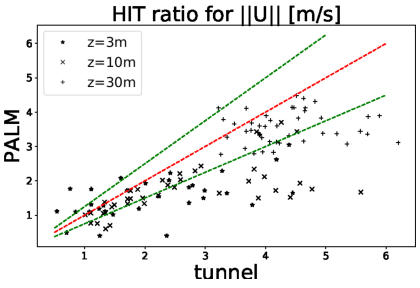

Fig. 8: Mean velocity magnitudes hit.

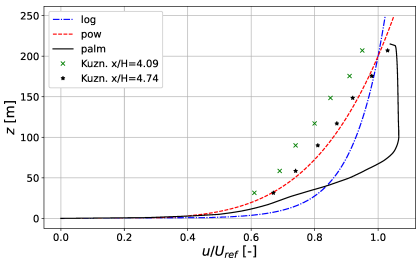

Fig. 9: Velocity profiles at the beginning of the test section.

inner domain. In the Fig. 9 the vertical profiles of u velocity in the tunnel axes in front the test section are plotted (at the distance $x/H = 4.74$). For illustration, two possible theoretical profiles are plotted in the graph as well as experimental profile at the different distance ($x/H = 4.09$). The profile from PALM (black line) behaves differently than the experimental profile (Kuzn. [3]).

The Fig. 10 displays a situation inside the test section for each point in height 30 m. The points are coloured according to formula

$$\left(\frac{u_{\text{palm}}}{u_{\text{exp.}}} - 1\right) \cdot 100\%,$$

which means how accurately they hit the experimental value. Some patterns can be identified in the figure, such that the velocities inside the closed building block fit well and the values in front of the closed building block are very underpredicted, but the rest seems quite random. That leads us to consideration of wrong turbulent structure in the simulation probably caused by lacking of right tools and information how to prescribe it at the inlet (as the results from the first experiment suggested).

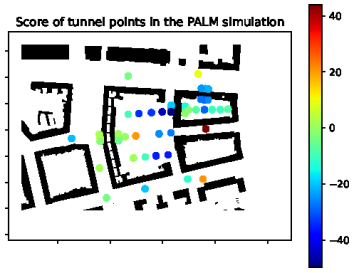

Fig. 10: Measuring points colored according $(u_{\text{palm}}/u_{\text{exp.}} - 1) \cdot 100\%$

Profile in the Fig. 9 reveals problems with different flow rate between simulated and measured profiles, but this issue can be related to the wrong top boundary condition. Or the upper boundary condition (the top of the computational domain) is simply placed too low to satisfy fully Dirichlet b.c. (without any inflow through upper boundary). Sadly the provided information from the validation data doesn't contained any velocities for higher heights (z-coordinate). Yet the data suggests the flow rate is changed between profiles - the first profile at $x/H = 4.09$ contains smaller velocities than the second one at $x/H = 4.74$ (at the beginning of inner domain). Therefore the flow rate to the numerical domain from above is unknown and it cannot be properly simulated.

The first numerical experiment at least confirmed that convergence of the model is achieved relatively quickly. As Fig. 11 shows, the steady state in terms of kinetic energy and resolved Turbulent Kinetic Energy (TKE) conservation is reached approximately after 15 min. of the simulation. The spectral density of TKE corresponds well to the Kolmogorov's cascade as plotted in the graph of Fig. 12.

The comparison of Turbulent Intensity (TI) profiles in the Fig. 13 for the PALM outputs and calibration measurement with hot-wire (in the tunnel axes ahead of the test section) indicates the good ability of the model to capture well the empty tunnel with roughness elements only (when the castellated barrier wall and the vortex generators weren't present). On the other hand the fully developed profiles of turbulence and velocity (will be described further) of the fully equipped wind tunnel (with all three elements generating similar flow to ABL) are difficult to get from the model. Probably they have to be prescribed as an inlet b.c. which includes the complete

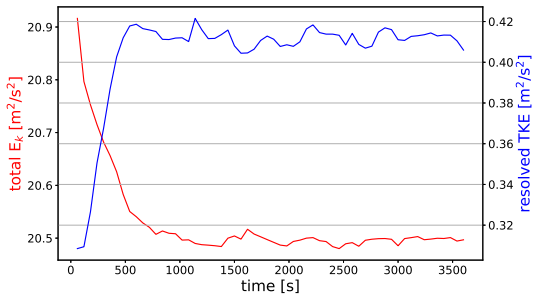

Fig. 11: Convergence for kinetic energy and Turbulent Kinetic Energy (TKE) conservation.

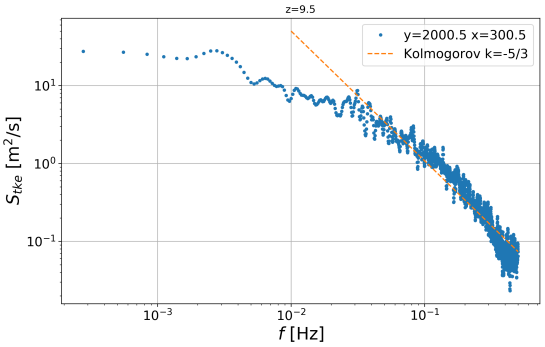

Fig. 12: Spectral density of resolved TKE.

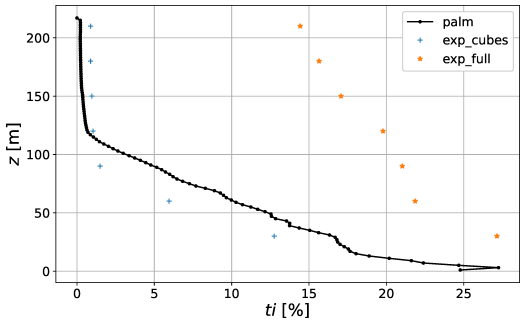

Fig. 13: Vertical profiles of Turbulent Intensity at the beginning of the test section.

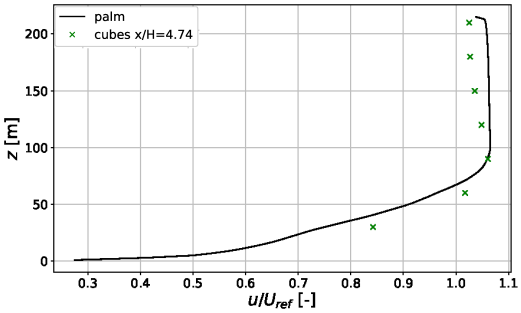

Fig. 14: Velocity profile compared to empty tunnel with roughness elements only (cubes).

information about turbulence structure. When the dimensionless velocity profiles are compared to the empty tunnel profiles with roughness elements (cubes) only in the Fig. 14, they fit quite well.

Other numerical experiments were conducted with the cyclic b.c. (inlet/outlet), different inputs (logarithmic law, power law) and with switching (ON/OFF) the turbulence disturbances at the inlet, but none of them led to systematical improvement. Even the simulation with artificial tunnel walls (by adding high buildings to sides) was tried but the changes were in terms of percents (and not systematically).

The last numerical experiment to be mentioned here used the known velocity profile to obtain results closer to the experiment. The power law velocity profile

$$u(z) = U_{\text{ref}} \left(\frac{z}{z_{\text{ref}}} \right)^{\alpha}, \tag{3}$$

with coefficient $\alpha = 0.22$ and $z_{\text{ref}} = 200$ m, was prescribed on the inlet. The turbulence on the inlet was generated by the disturbances (without synthetic turbulent generator). As shown in Fig. 15 the profile still doesn't match fully developed state. The flow is decelerated near the ground much more than expected.

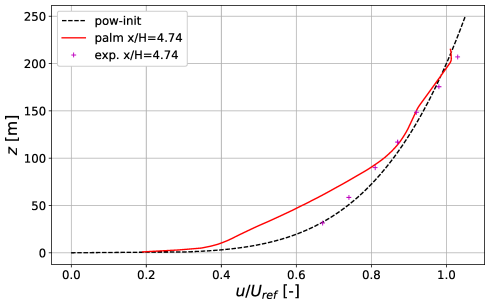

Fig. 15: Velocity profiles for the second numerical experiment.

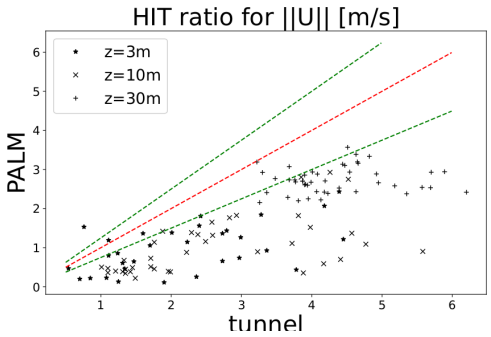

Fig. 16: Mean velocity magnitudes.

The hit ratio in that case is even worse as is indicated in the Fig. 16. However, it is not surprising because the simulated flow entering the testing domain in this case is much slower than the physical flow in the wind-tunnel.

5. Conclusions

A big simulation (containing circa 25×10^8 cells) of the whole wind-tunnel atmospheric section was performed by atmospheric LES model PALM and its results were compared to the measurements. It was shown that kinetic energy conservation is achieved relatively quickly and the calculated turbulence spectrum corresponds to the theory. The results obtained for the "naive" uniform initial velocity profile were promising but not satisfying. The model was able to develop the correct profile over the roughness elements without vortex spikes and castellated barrier wall quite well in the case of velocity and even of turbulent intensity.

The reproduction of ABL is a challenging question even for smaller scales and well defined condition of a wind tunnel. Based on the data provided by the validation paper the model PALM is unable to reproduce the fully developed wind profile with correctly generated turbulence structures. It leads to strong under-estimation of the velocities inside the street canyon. The measurement of the main flow should be provided much higher or the flow rate through top boundary should be known. As is shown PALM can reproduce the boundary layer created with the roughness cubes only. For recreation of the boundary layer produced by the other elements (vortex spikes and castellated barrier wall) the complete recirculation zone measurements is probably needed and the top boundary of the computing domain has to be probably placed much higher. To conclude that the results of the model are limited with prescription of correct turbulent structure and the known (well developed) velocity profile. Unfortunately, such profile wasn't provided by the experimenters and during our numerical experiments it wasn't found. The question, how to impose the correct profile (even if we know it), remains for the future testing.

The future endeavors are pointed to the simulation of cyclic domain (infinite) with smaller part serving as precursor where the correct profile could be developed.

Also we hope that we can adopt some knowledge obtained by testing original code provided by [2]. If it was possible we would ask for the new measurements with the empty tunnel with roughness elements only to see whether the well defined inlet improved our hit ratio.

Acknowledgements

This work was supported by the Strategy AV21 projects "Energy interactions of buildings and the outdoor urban environment" and "City as a Laboratory of Changes", financed by the Czech Academy of Sciences. The data post-processing was possible due to the student grant SGS22/148/OHK2/3T/12 of the Czech Technical University in Prague.
The measurements were possible due to the support of grant GACR 22-08786S financed by The Czech Science Foundation (GACR). The 3D-geometry for the model was kindly provided by Operátor ICT, a.s. (operatorict.cz).

References

[1] Baldauf, M.: Stability analysis for linear discretisations of the advection equation with Runge–Kutta time integration. Journal of Computational Physics **227** (2008).

[2] Gronemeier, T. et al.: Evaluation of the dynamic core of the PALM model system 6.0 in a neutrally stratified urban environment: comparison between LES and wind-tunnel experiments. Geoscientific Model Development **14** (2021).

[3] Kuznetsov, S. et al.: Flow and turbulence control in a boundary layer wind tunnel using passive hardware devices. Experimental Techniques **41** (2017).

[4] Maronga, B. et al.: The parallelized large-eddy simulation model (PALM) version 4.0 for atmospheric and oceanic flows: model formulation, recent developments, and future perspectives. Geoscientific Model Development **8** (2015).

[5] Resler, J. et al.: Validation of the PALM model system 6.0 in a real urban environment: A case study in Dejvice, Prague, the Czech Republic. Geoscientific Model Development **14** (2021).

[6] Wicker L. J., S. W.: Time-splitting methods for elastic models using forward time schemes. Mon. Weather Rev. **130** (2002).